SUPPLEMENT

Chromophore Hydrolysis and Release from Photoactivated Rhodopsin in Native Membranes

John D. Hong[1,2], David Salom[1], Michał Andrzej Kochman[3], Adam Kubas[3], Philip Kiser[1,4,5,6], Krzysztof Palczewski[1,2,4,7]*

[1] Gavin Herbert Eye Institute, Department of Ophthalmology, Gavin Herbert Eye Institute, University of California Irvine, Irvine, CA 92697, USA

[2] Department of Chemistry, University of California Irvine, Irvine, CA 92697, USA

[3] Institute of Physical Chemistry, Polish Academy of Sciences, Kasprzaka 44/52, 01-224 Warsaw, Poland

[4] Department of Physiology and Biophysics, University of California Irvine, Irvine, CA 92697, USA

[5] Department of Clinical Pharmacy Practice, University of California Irvine, Irvine, CA 92697, USA

[6] Research Service, VA Long Beach Healthcare System, Long Beach CA, 90822, USA

[7] Department of Molecular Biology and Biochemistry, University of California Irvine, Irvine, CA 92697, USA

Corresponding Author:
Krzysztof Palczewski, Department of Ophthalmology, Gavin Herbert Eye Institute, UCI, Irvine, CA 92697; kpalczew@uci.edu; phone (949) 824-6527

Table of Content

Instrumentation

1100 Series HPLC System (Agilent, Santa Clara, CA); 1260 Infinity HPLC System (Agilent); Dionex Ultimate 3000 UHPLC System (Thermo Fisher Scientific, Waltham, MA); LTQ XL mass spectrometer (Thermo Fisher Scientific); Cary 50 UV-Vis Spectrophotometer (Varian, Palo Alto, CA).

Materials

Chemicals and other materials were purchased as follows: all-*trans*-retinal (Sigma-Aldrich, St. Louis, MO, cat. no. R2500), all-*trans*-retinol (Sigma-Aldrich, cat. no. R7632); bovine rod outer segments (InVision Bioresources, Seattle, WA, cat. no. 98740); 2-[4-(2-hydroxyethyl)piperazin-1-yl]ethanesulfonic acid (Goldbio, St. Louis, MO, cat. no. H-400-1); 1,3-Bis[tris(hydroxymethyl)methylamino]propane (Sigma-Aldrich, cat. no. B6755); calcium chloride dihydrate (Sigma-Aldrich, cat. no. 223506); n-dodecyl-β-D-maltopyranoside Sol-grade (Anatrace, Maumee, OH, cat. no. D310S); Amicon Ultra-0.5 Centrifugal Filter (Millipore, Burlington, MA, cat. no. UFC503096); acetonitrile Optima LC/MS grade (Fisher Scientific, Pittsburgh, PA, cat. no. A955); MeOH Optima LC/MS grade (Fisher Scientific, cat. no. A456); *i*PrOH Optima LC/MS grade (Fisher Scientific, cat. no. A461); formic acid Optima LC/MS grade (Fisher Scientific, cat. no. A117-50); methylene chloride (HPLC) (Fisher Scientific, cat. no. D143); hexanes (HPLC) (Fisher Scientific, cat. no. H302); ethyl acetate (HPLC) (Fisher Scientific, cat. no. E195); triethylamine (HPLC) (Fisher Scientific, cat. no. O4884); dimethyl sulfoxide (Sigma-Aldrich, cat. no. D2650); N,N-dimethylformamide (Fisher Scientific, cat. no. AC327171000); diethylamine (Sigma-Aldrich, cat. no. 471216); N^{α}-[(9H-fluoren-9-ylmethoxy)carbonyl]-L-Lys hydrochloride (Fisher Scientific, cat. no. F0586); 1,2-dioleoyl-sn-glycero-3-phosphoethanolamine (Avanti Polar Lipids, Alabaster, Al, cat. no. 850725P); $NaBH_4$ (Alfa Aesar, Haverhill, MA, cat. no. 88983); $NaBD_4$ (Alfa Aesar, cat. no. 35102); Isotemp 3016S Water Bath (Fisher Scientific, cat no. 13-874-28); 85 W 2700 K Hg light bulb (Home Depot, cat. no. EDXR-40-19); Fiber-Coupled 565 nm 9.9 mW (Min) 700 mA LED (Thorlabs, Newton, NJ, cat. no. M565F3); Fiber Patch Cable (Thorlabs, cat. no. M92L01); Compact T-Cube 1200 mA LED Driver with Trigger Mode (Thorlabs, cat. no. LEDD1B); Power Supply Unit with 3.5 mm Jack Connector (Thorlabs, cat. no. KPS201); HPLC columns: BioPureSPN C18 TARGA (nestgrp, Ipswich, MA cat. no. HEM S18R); XBridge C18 (Waters, Milford, MA, 2.1 mm X 100 mm, cat. no. 186003022); Gemini Analytical C18 (Phenomenex, Torrance, CA, 250 x 4.6 mm, cat. no. 00G-4435-E0); Gemini Preparatory C18 (Phenomenex, 250 x 10 mm, cat. no. 00G-4435-N0); Luna Preparatory Silica (Phenomenex, 250 x 21.2 mm, cat. no. 00G-4091-P0-AX).

Supplementary methods

Production of 9-*cis*-, 11-*cis*-, and 13-*cis*-retinal. The method for production of 9-*cis*-retinal, 11-*cis*-retinal, and 13-*cis*-retinal was adapted from Kahremany *et al.* (1). Thus, all-*trans*-retinal was solubilized in ACN at 0.2 M and illuminated with an 85 W Hg light bulb at maximum intensity at a distance of 10 cm for 12 hr at 4 °C. The resultant 9-*cis*-, 11-*cis*-, and 13-*cis*-retinal products were purified with a Luna preparatory silica column using 90% hexane and 10% ethyl acetate as the mobile phase at a flow rate of 5 mL/min. The purified products were verified by comparison to standards.

Synthesis of N^{ε}-retinyl-Lys Standards. N^{α}-Fmoc-L-Lys HCl (15 mg) was dissolved in 0.25 mL dimethylformamide (DMF). Under dim red light in the dark room, 5.25 mg (0.5 eq.) of a retinal isomer (9-*cis*-, 11-*cis*-, 13-*cis*-, or all-*trans*-retinal) in 0.25 mL DMF was added to the DMF solution of Nα-Fmoc-L-Lys. Then 2.6 µL triethylamine (0.5 eq.) was added to the mixture and incubated for 6 hr. Then, about 2 mg of $NaBH_4$ was added, followed by 0.25 mL MeOH. About 3 min later, 0.5 mL diethylamine was added for Fmoc deprotection, and the reaction mixture was incubated for another 30 min. The reaction mixture was concentrated to 0.4 mL under a gentle stream of nitrogen. Then, 0.3 mL 1 M HEPES (pH 7.4) was added slowly to quench excess $NaBH_4$ and to neutralize the reaction mixture. The resultant suspension was centrifuged at 20,000 x g for 1 min. The resultant crude product in the supernatant was purified using a Gemini preparatory C18 column and a 30-min gradient of 10% to 40% ACN in water with 0.1% FA at a flow rate of 3 mL/min. Depending on the retinal isomer used (9-*cis*-, 11-*cis*-, 13-*cis*-, or all-*trans*-retinal), the corresponding retinyl isomer of the N^{ε}-retinyl-Lys product was purified and characterized by UV-Vis spectrometry and MS.

Synthesis of N-retinyl-dioleoylphosphatidylethanolamine standard.
Dioleoylphosphatidylethanolamine (DOPE, 100 mg) was dissolved in 4 mL of 4:1 methylene chloride:MeOH. Under dim red light in a dark room, 50 mg of all-*trans*-retinal (1.3 eq.) dissolved in 1 mL of methylene chloride was added to the solution of DOPE. Subsequently, 18.7 µL of triethylamine (1 eq.) was added, and the reaction mixture was left to incubate in the dark room overnight. The reaction mixture was concentrated to 0.5 mL under a gentle stream of nitrogen. 200 µL DMF and 200 µL MeOH were added, the mixture was re-concentrated to ~0.4 mL, and then centrifuged at 20,000x g for 1 min. The supernatant was chromatographed using a Gemini preparatory C18 column and a mobile phase consisting of water with 0.1% FA (solvent A) and MeOH with 0.1% FA (solvent B). The conditions were as follows: a 10-min gradient of 95% to 100% solvent B, followed by a 20-min isocratic gradient of 100% solvent B at a flow rate of 3

mL/min. The only peak with a λ_{max} of 450 nm, characteristic of N-retinylidene-DOPE, was collected into a vial on ice containing 3 mg of $NaBH_4$. Any excess $NaBH_4$ was quenched by 10 µL additions of 1 M ammonium acetate until no further bubbling was observed. The resultant reduced product was concentrated to 0.2 mL under a gentle stream of nitrogen and chromatographed using the same HPLC conditions to purify the dominant peak at 330 nm, which was confirmed to be N-retinyl-DOPE by MS/MS, using CID fragmentation.

Synthesis of N$^{\varepsilon}$-at-retinyl-bRhoPep. The peptide of bovine Rho, bRhoPep, encompassing the amino acid sequence 292 to 302 with an N-terminal acetylation modification was synthesized by Genscript. Four mg of the bRhoPep was dissolved in 200 µL dimethyl sulfoxide. 2 mg (~2.2 eq.) all-*trans*-retinal was dissolved in 200 µL dimethyl sulfoxide and added to the peptide solution. Approximately 1 µL of triethylamine was added to help deprotonate the ε amino group of Lys^{296} of bRhoPep. The reaction was incubated for 12 hr; an excess of $NaBH_4$ (1 mg, ~8.3 eq.) was added to reduce the SB condensate, followed by 400 µL of MeOH. To quench the remaining $NaBH_4$, 200 µL of 1 M ammonium acetate was added slowly. The reaction mixture was concentrated to 400 µL using a stream of nitrogen gas. The concentrated mixture was centrifuged at 20,000 x g for 1 min. The product was purified from the supernatant by HPLC using a Gemini analytical C18 column and a mobile phase consisting of water with 0.1% FA (solvent A) and ACN (solvent B). The method consisted of a single 25-min isocratic gradient of 40% solvent B at a flow rate of 1 mL/min. The prominent peak with λ_{max} of 328 nm was collected and the identity of the product was confirmed using LC-MS/MS. The ACN in the purified N$^{\varepsilon}$-a*t*-retinyl-bRhoPep was partially evaporated by a stream of nitrogen, concentrating about 1 mL of N$^{\varepsilon}$-a*t*-retinyl-bRhoPep solution collected directly from the HPLC to 0.5 mL. The concentration of N$^{\varepsilon}$-a*t*-retinyl-bRhoPep was measured to be around 50 mM *via* UV-Vis spectrometry, using the extinction coefficient of all-*trans*-retinol (ε = 52,800 M^{-1} cm^{-1} at λ_{max} = 325 nm).

Pronase Digest of N$^{\varepsilon}$-a*t*-retinyl-bRhoPep. 50 µL of 50 mM N$^{\varepsilon}$-a*t*-retinyl-bRhoPep was mixed with 100 µL of 1 M BTP pH 7.8 and 100 µL of 1 M $CaCl_2$. The entire mixture was adjusted to 1 mL final volume with nanopure water. Finally, 1 µL of 40 mg/mL pronase was added and the digestion was incubated for 4 hr at 40 °C in the dark. The digest was passed through a BioPureSPN C18 spin column for desalting. The column was washed with 20% ACN, and digest products were eluted using 50% ACN. The eluted N$^{\varepsilon}$-retinyl-Lys products were separated using a Dionex UHPLC with a XBridge C18 column and a 30 min gradient of 20% to 50% ACN in water with 0.1% FA at a flow rate of 0.3 mL/min. N$^{\varepsilon}$-retinyl-Lys products were detected by

UHPLC absorbance readings at 330 nm and identified by MS/MS, using CID fragmentation with the LTQ XL spectrometer.

Proteinase K Digest of N$^{\varepsilon}$-a*t*-retinyl-bRhoPep. 50 µL of 50 mM N$^{\varepsilon}$-a*t*-retinyl-bRhoPep was mixed with 100 µL of 1 M BTP pH 7.8 and 100 µL of 1 M $CaCl_2$. The entire mixture was adjusted to 1 mL final volume with nanopure water. Finally, 1 µL of 20 mg/mL proteinase K was added and the digestion was incubated for 4 hr at room temperature in the dark. The digest was passed through a BioPureSPN C18 spin column for desalting. The column was washed with 20% ACN, and digest products were eluted using 60% ACN. The eluted N$^{\varepsilon}$-retinyl-peptide products were separated on the Dionex UHPLC with a XBridge C18 column and a 30 min gradient of 20% to 50% ACN in water with 0.1% FA at a flow rate of 0.3 mL/min. N$^{\varepsilon}$-retinyl-peptide products were detected by UHPLC absorbance readings at 330 nm and identified by MS/MS, using CID fragmentation with the LTQ XL spectrometer.

Kinetic studies of N-ret-PE formation. In the dark room under dim red light, ROS membranes (2 mg/mL or 50 µM Rho) were prepared as a suspension in 20 mM HEPES-buffered solution at pH 5.6, 7.4, or 8.3. The reaction between a*t*RAL and ROS lipids was initiated upon addition of 2.5 molar equivalents of a*t*RAL relative to the amount of Rho within the ROS. The reaction was performed in an isothermal water bath set to 20 °C. To 1 part ROS membranes, 3 parts saturated solution of $NaBH_4$ granules (about 100 µM) in cold *i*PrOH was added at different time-points after the addition of a*t*RAL. Lipids solubilized by the *i*PrOH were analyzed by analytical reverse-phase HPLC, as described above. The molar quantity of free a*t*RAL (reduced to a*t*ROL) was determined from a standard curve generated with a*t*ROL standard. The molar quantity of N-ret-PE products (reduced to N-retinyl-PE) was determined from a standard curve generated with synthetic N-retinyl-DOPE. The rate of formation of N-ret-PE was determined by plotting the mole fraction of N-ret-PEs over the total molar amount of free and PE-bound a*t*RAL at each time-point.

Kinetic studies of N-ret-PE formation following Rho* hydrolysis. A suspension of ROS (2 mg/mL or 50 µM Rho) in 20 mM HEPES (pH 7.4) buffered solution was illuminated with 565 nm fiber light for 10 sec at an intensity of 625 µW. The illuminated ROS membranes were incubated in the dark in an isothermal water bath at various temperatures (15, 20, 25, 31, and 37 °C). To 1 part ROS membranes, 3 parts saturated solution of $NaBH_4$ granules (about 100 µM) in cold *i*PrOH was added at different time-points to halt any further Rho* hydrolysis and any further SB condensation reaction between a*t*RAL and PE. Lipids solubilized by the *i*PrOH were analyzed by analytical reverse-phase HPLC to determine the kinetics of N-ret-PE formation as described

above. The kinetics of N-ret-PE formation was determined also as described above. The rate of the formation of N-ret-PE was determined by plotting the mole fraction of N-ret-PEs over the total molar amount of free and PE-bound a*t*RAL produced from Rho* hydrolysis at each time-point.

Kinetic studies of Rho* hydrolysis. Aliquots of the same ROS samples treated with $NaBH_4$ in *i*PrOH (described above for tracking N-ret-PEs formed from a*t*RAL released from hydrolyzed Rho*) were used to obtain the protein precipitate, which was digested with pronase to produce N$^{\varepsilon}$-retinyl-Lys as described in the main text. The resultant N$^{\varepsilon}$-retinyl-Lys products were analyzed chromatographically using an Agilent 1260 Infinity HPLC system with a XBridge C18 column and an 18-min gradient of 30% to 39% ACN in water with 0.1% FA at a flow rate of 0.3 mL/min. N$^{\varepsilon}$-retinyl-Lys products were detected by HPLC absorbance at 330 nm and identities were confirmed by MS/MS as described above. The molar quantity of each isomer of N$^{\varepsilon}$-retinyl-Lys (9-*cis*, 11-*cis*, 13-*cis*, and *all-trans*) was determined based on a standard curve generated using synthetically produced N$^{\varepsilon}$-retinyl-Lys isomers. The mole fraction of opsin-bound retinal (measured as moles of N$^{\varepsilon}$-retinyl-Lys) over the total retinal content (measured as the sum of the moles of N$^{\varepsilon}$-retinyl-Lys and the moles of a*t*RAL produced from Rho* hydrolysis, determined above when analyzing N-ret-PE formation kinetics) was plotted for each time-point, generating a curve which was consistent with pseudo first order decay kinetics. An Arrhenius plot (-ln(*k*) vs T; equation $k = \mathrm{A}e^{-\mathrm{E_A/RT}}$; linearized equation $\ln(k) = -\frac{E_A}{RT} + \ln(\mathrm{A})$) was generated based on hydrolysis rate constants (*k*) determined at each temperature(15, 20, 25, 31, and 37 °C) to yield the E_A based on the slope of the Arrhenius curve ($m = -\mathrm{E_A/R}$ or $\mathrm{E}_A = -m\mathrm{R}$, where $m = \mathrm{slope}$ and $R = \mathrm{gas\ constant}$).

pH studies of Rho* hydrolysis and subsequent N-ret-PE formation. The same kinetic studies of both reactions as described above were repeated at 20 °C, using buffers adjusted to pH 5.6 and pH 8.3, to obtain rate constants at each pH value.

Rho immunopurification from ROS membranes. Rho was immunopurified in a dark room under dim red light, using immobilized 1D4 antibody as previously described (2). ROS membranes were solubilized with DDM in 20 mM HEPES at pH 7.4 with 0.15 M NaCl and incubated with Sepharose beads with immobilized 1D4 antibody for 2 hr. The beads were washed with 10 column volumes of wash buffer A (1 mM DDM in 20 mM HEPES pH 7.4, 0.15 M NaCl) to remove unbound protein as well as solubilized lipids. Rho was then eluted from the beads by adding a 0.5 mM solution of the competing peptide TETSQVAPA (1D4), which was

subsequently removed by membrane filtration using a 30 kDa Amicon centrifugal filter. The Rho sample was then concentrated and diluted twice with wash buffer B (0.2 mM DDM, 20 mM HEPES pH 7.4). The final concentration was 2 mg/mL Rho in 20 mM HEPES in roughly 0.5 mM DDM.

Kinetic studies of hydrolysis of detergent-solubilized Rho* and subsequent formation of N-ret-PE. Using immunoaffinity-purified Rho depleted of lipid content and solubilized in DDM detergent, kinetic studies of Rho* hydrolysis and N-ret-PE formation analogous to those described above were conducted at pH 7.4 and 20 °C to obtain rate constants. The rates for detergent-solubilized Rho were compared to those for Rho in ROS membranes.

Quantum chemical calculations. Calculations were performed on a cluster model of the Rho active site that was extracted from the X-ray crystal structure (PDB accession code: 3PQR) (3). This structure is interpreted to correspond to the MII state. We note that the active site pocket of Rho remains unchanged among various structures reported for all-*trans* Rho. We included all residues within 6 Å of the a*t*RAL chromophore (*SI Appendix*, Figure S9). The free valences were saturated with hydrogen atoms. The active site was filled with an additional eight water molecules that saturate H-donors/acceptors, including Glu residues and the N^{ε} atom of the a*t*RSB. The size of such a model (ca. 550 atoms) is too large to carry out full quantum chemical (QM) optimizations, so we decided to carry out two-level hybrid QM1-QM2 calculations, where QM1 and QM2 denote high-level and low-level QM methods, respectively. Accordingly, the positions of the carbonyl carbon atoms of the residues that comprise the active site pocket were frozen. We refer here to Figure S9 for the list of QM residues and indices of the fixed atoms. The calculations were carried out within the density functional theory approach (DFT), with the recently developed robust r2SCAN functional and def2-TZVP basis set as the QM1 method and the tight-binding DFT method GFN2-xTB as the QM2 economic method (4-6). The cluster's environment was simulated with the analytical linearized Poisson-Boltzmann (ALPB) model (7). Protonation energy **IIc** $\rightarrow$ **IId** was estimated as the change in energy in the following reaction: **IIc** + $(H_3O^+)(H_2O)_3 \rightarrow$ **IId** + $(H_2O)_4$. Numerical partial Hessian calculations were performed at the QM1 atoms to obtain estimates of the zero-point energies (ZPE) and confirm the nature of the located states. The final values reported throughout the manuscript are ZPE-inclusive. All calculations were performed with the ORCA 5.0.2 program coupled to Grimme's standalone xtb 6.4 code (8, 9). XYZ coordinates of all structures reported can be accessed free of charge via RepOD repository: https://doi.org/10.18150/9HP0S1

Monitoring a*t*RAL reduction by RDHs using LC-MS. The visual cycle occurring in the outer segment starting from the hydrolytic release of a*t*RAL from Rho* to the formation of N-ret-PEs and ultimate reduction of a*t*RAL by RDHs can be tracked with the use of $NaBD_4$ (*SI Appendix*, Fig S10). Treatment of 1 part ROS membranes (2 mg/mL or 50 μM Rho) with 3 parts saturated $NaBD_4$ in cold ethanol (EtOH) effects essentially the same outcomes as with $NaBH_4$ (described above), reducing Rho*-hydrolyzed, Rho*-bound and PE-bound a*t*RAL; however, in this case each species is labeled with a deuterium as shown in Fig. S10. A*t*RAL reduced by NADPH produces a*t*ROL, whereas a*t*RAL reduced by $NaBD_4$ produces C^{15}-D^1-a*t*ROL. A*t*ROL and C^{15}-D^1-a*t*ROL can be distinguished by MS and detected by tracking their ESI source-fragmentation retinyl cation products with m/z ratios of 269 and 270, respectively. The percentage of 269 m/z signal intensity was calculated relative to the total signal intensity from the 269 and 270 m/z peaks in each sample and normalized to the natural-abundance percentage of 269 m/z signal in in the C^{15}-D^1-a*t*ROL standards, representing no reduction of a*t*RAL by NADPH and RDHs; or to the natural-abundance percentage of 269 m/z signal in the a*t*ROL standards, representing complete reduction of all of the a*t*RALs. Thus, the normalized percentage of 269 m/z signal in a sample indicates the amount of free a*t*RAL reduced by NADPH and RDHs. Any N-ret-PEs observed in ROS membranes were treated as a*t*RAL unreduced by RDHs. RDH activity was thereby captured by tracking both the proportion of a*t*RAL bound as N-ret-PE and the percent of free a*t*RAL reduced by RDHs with NADPH.

In the dark room under dim red light, ROS membranes (2 mg/mL or 50 μM Rho) were prepared in 20 mM HEPES at pH 7.4 with 250 μM dinucleotide, either NADP or NADPH; or 250 μM NaCl, control. Then membranes were illuminated with a 565 nm fiber light at 625 μW for 10 sec followed by incubation at 20 °C. To 1 part ROS membranes, 3 parts saturated solution of $NaBD_4$ in cold EtOH was added at 0, 8, and 16 min after illumination. The extent of Rho* hydrolysis yielding a*t*RAL and the proportion of released a*t*RAL bound to PE were determined as described previously. The extent of subsequent a*t*RAL reduction by RDHs was determined also as described above.

To track RDH activity in the presence of pre-formed N-ret-PE, ROS membranes (2 mg/mL or 50 μM Rho) were prepared in 20 mM HEPES at pH 7.4 and spiked with 4 molar equivalents of a*t*RAL relative to the amount of Rho. After 16 min incubation with a*t*RAL, NADPH was added in excess for a final concentration of 500 μM and mixed by gentle vortex agitation. The reduction was tracked by adding 3 parts saturated solution of $NaBD_4$ in cold EtOH to 1 part ROS membranes at various time-points up to 32 min after addition of NADPH. The extent of a*t*RALs

reduced by RDHs was determined also as described above by measuring the proportion of PE-bound a*t*RAL and the proportion of free a*t*RAL reduced by RDHs, as indicated by the percentage of 269 m/z signal.

Supplementary Figures

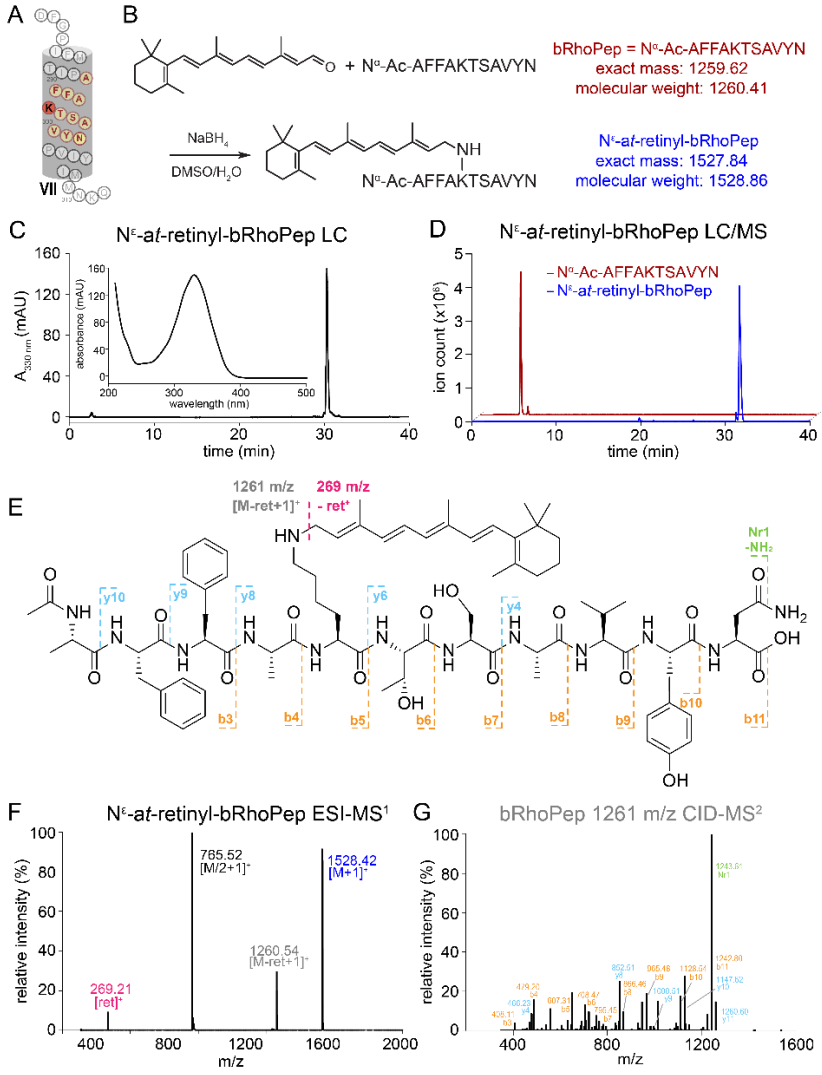

Figure S1. Synthesis and characterization of Nε-*at*-retinyl-bRhoPep. (A) Location of bRhoPep sequence within helix VII of bRho. (B) Synthesis of Nε-*at*-retinyl adducted to Lys[296] of the bRhoPep *via* $NaBH_4$-reduction of the a*t*RAL-bRhoPep SB. (C) HPLC chromatogram indicating high purity of the synthesized Nε-a*t*-retinyl-bRhoPep, displaying the characteristic retinyl UV-Vis absorbance spectrum. (D) LC-MS chromatogram showing that the retinyl adduct greatly increased the overall hydrophobicity of the peptide. (E) Diagram of the observed LC-MS/MS ESI source and CID fragmentation pattern of Nε-a*t*-bRhoPep. (F) ESI-MS[1] showed source fragmentation of Nε-*at*-retinyl-bRhoPep (1528 m/z) with cleavage at the site of the retinyl adduct, producing a product retinyl cation (269 m/z) and a product peptide ion (1261 m/z). (G) CID fragmentation of the product peptide ion showed the characteristic peptide fragmentation pattern of bRhoPep as diagrammed in (E).

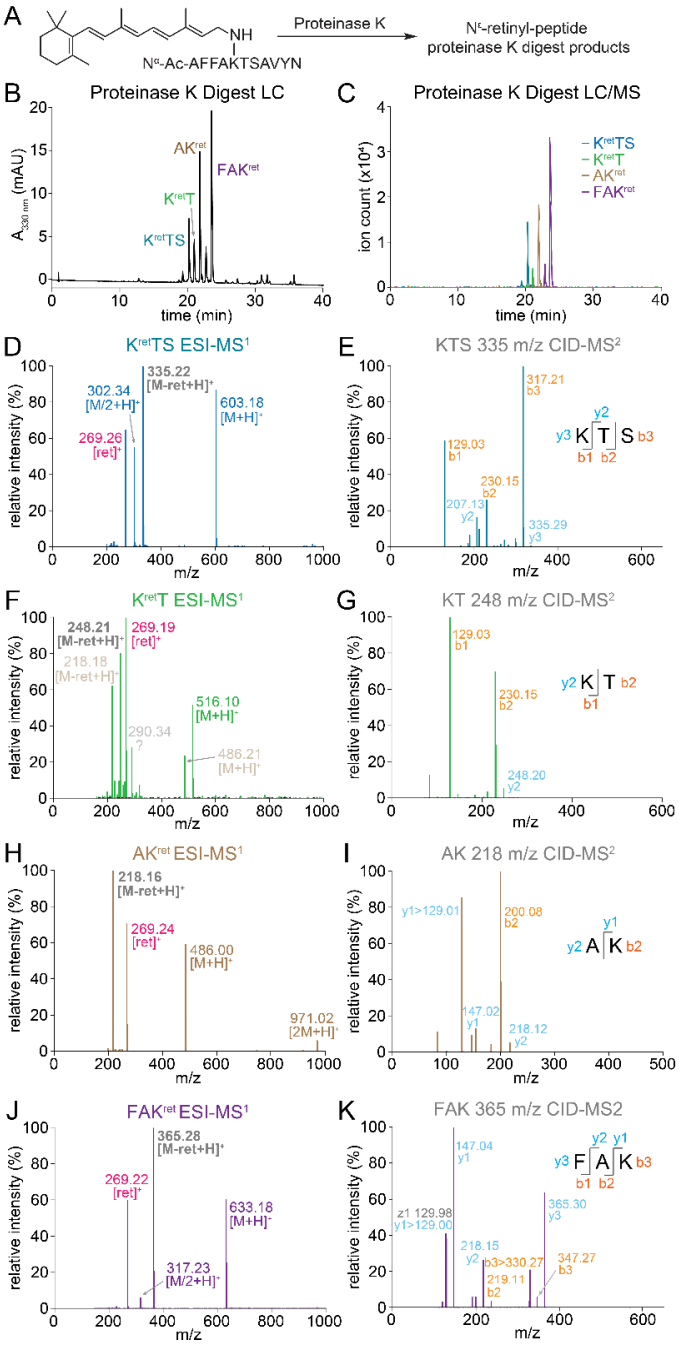

Figure S2. Proteinase K digestion of Nᵋ-*at*-retinyl-bRhoPep. (A) Schematic diagram of sample preparation and MS workflow. (B) Chromatogram of peptides displaying UV absorbance at 330 nm; *i.e.*, Nᵋ-a*t*-retinyl-peptides. (C) LC-MS chromatogram of various retinyl-peptides that were identified by MS/MS. (D, F, H, J) ESI-MS^1 full scans showed characteristic source fragmentation of the precursor Nᵋ-retinyl-peptide analytes to the product retinyl cation (269 m/z) and a product peptide ion. (E, G, I, K) Peptide sequences were determined by CID-MS^2 of each product peptide ion.

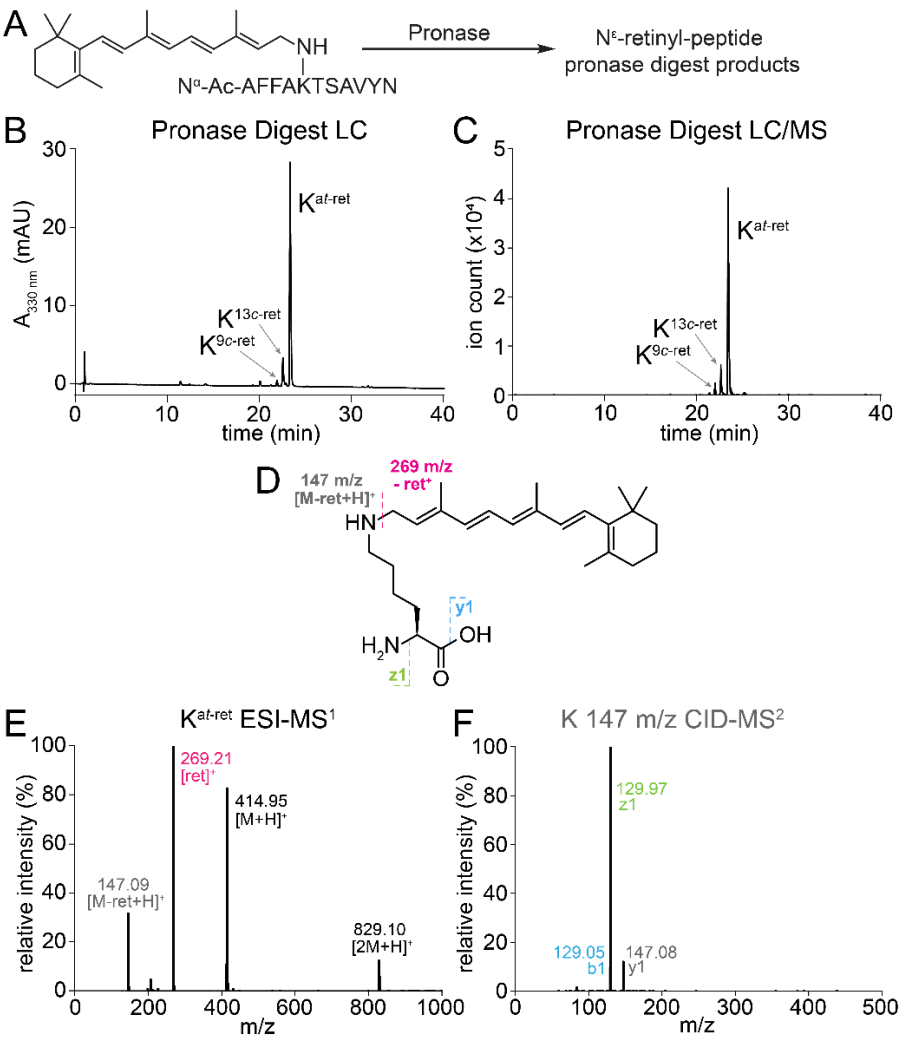

Figure S3. Pronase digest of Nε-*at*-retinyl-RhoPep. (A) Schematic diagram of sample preparation and MS workflow. (B) Chromatogram to detect Nε-*at*-retinyl-Lys *via* UV absorbance at 330 nm. (C) LC-MS chromatogram of Nε-retinyl-Lys digest product that was identified by MS/MS. (D) Diagram of LC-MS/MS fragmentation sites on Nε-retinyl-Lys. (E) ESI-MS^1 showing characteristic source fragmentation of precursor Nε-retinyl-Lys analyte (415 m/z) to a product retinyl cation (269 m/z) and product Lys ion (147 m/z). (F) CID-MS^2 of the product Lys ion showed the characteristic fragmentation pattern of Lys.

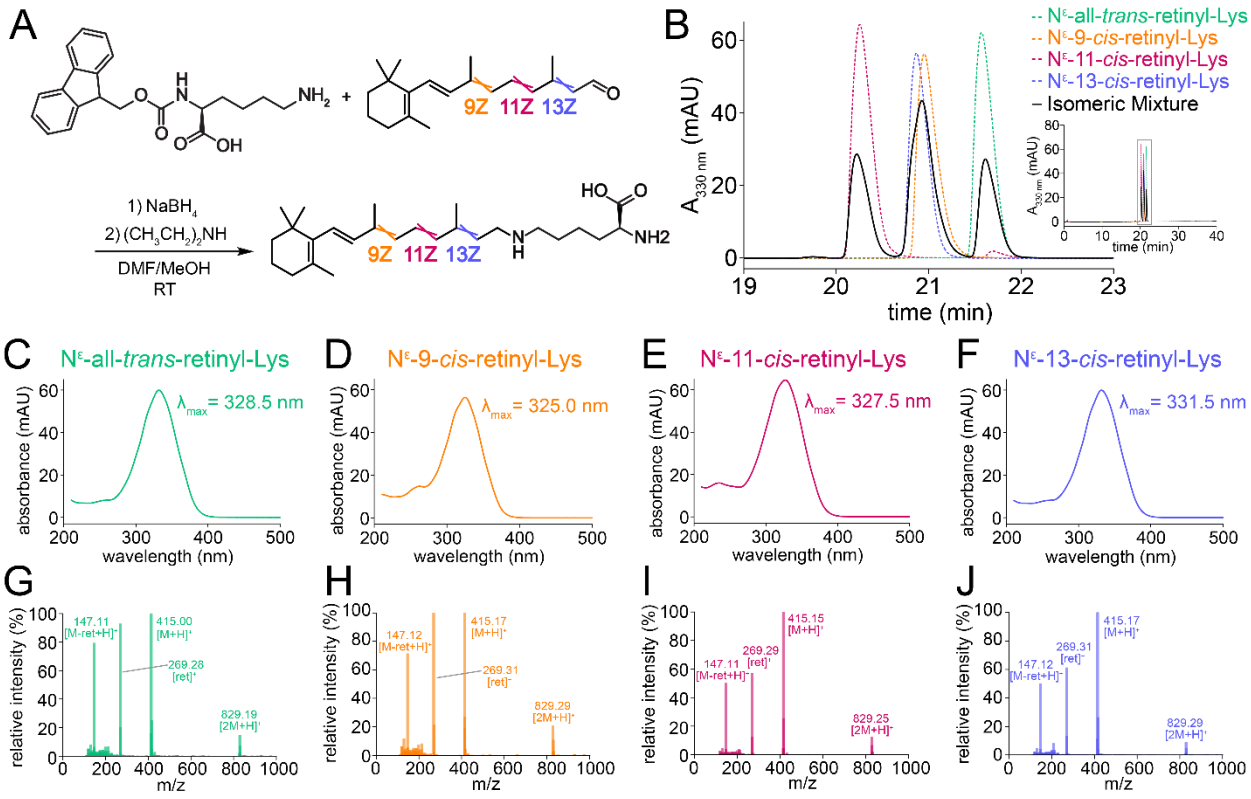

Figure S4. Development of a method for synthesis and separation of Nᵋ-retinyl-Lys standards. (A) Nᵋ-retinyl-Lys standards were synthesized by $NaBH_4$-reduction of the SB adducts of the different isomers of retinal with Nᵅ-Fmoc-Lys, followed by Fmoc deprotection using diethylamine. (B) Reverse-phase HPLC traces of each Nᵋ-retinyl-Lys isomer standard displayed separability of the 11-*cis* and all-*trans* isomer standards, demonstrating applicability in studying Rho photochemistry. (C-F) The UV-Vis spectrum of each Nᵋ-retinyl-Lys isomer standard showed unique spectral characteristics, especially the 9-*cis* and 13-*cis* isomers, which were poorly separable by chromatography but were spectrally the most distinct from each other. (G-J) ESI-MS^1 of each isomer demonstrated a source-fragmentation pattern characteristic of a retinyl moiety, with cleavage of the retinyl cation (269 m/z) from the precursor Nᵋ-retinyl-Lys ion (415 m/z) producing a product Lys ion (147 m/z).

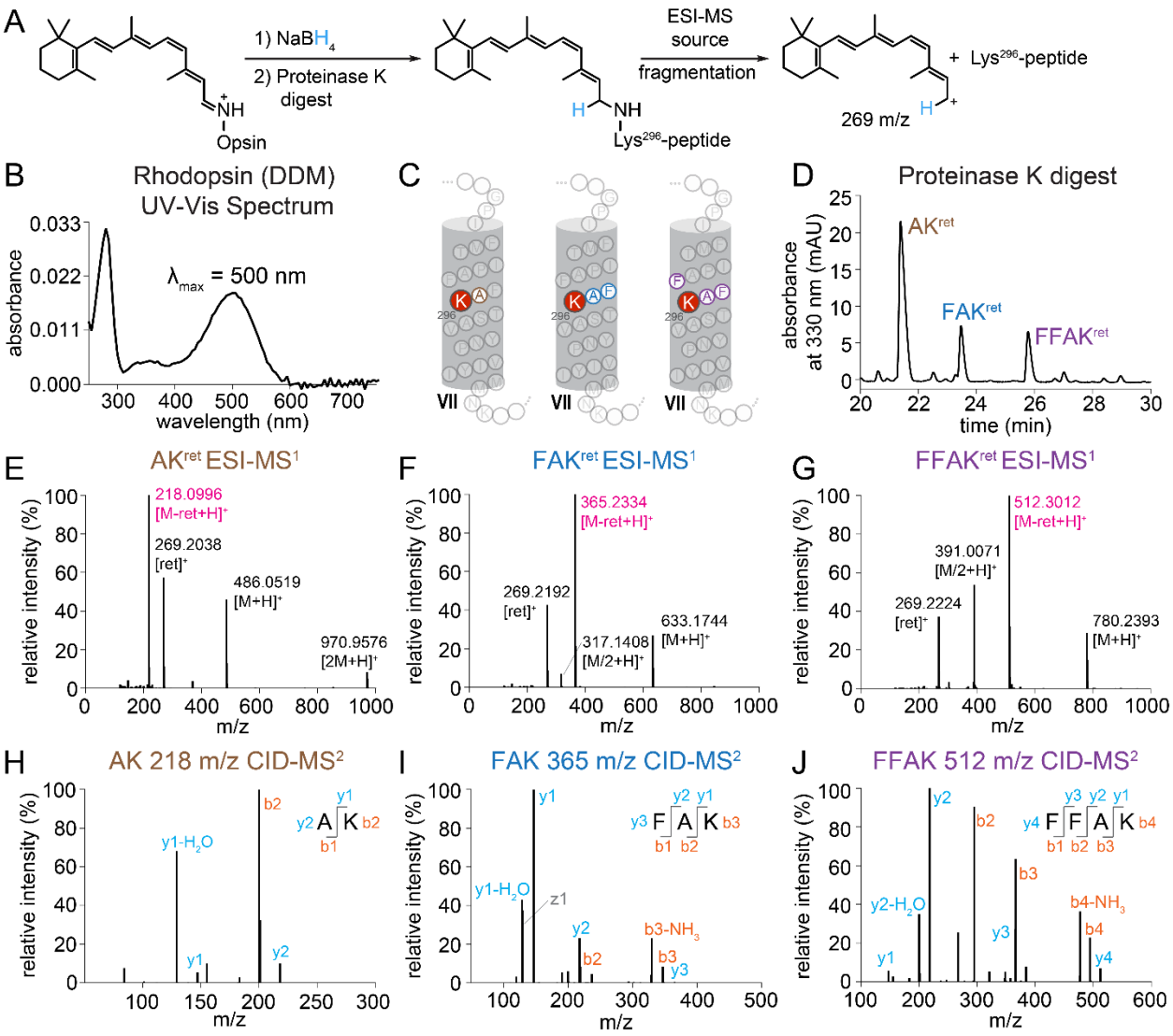

Figure S5. LC-MS/MS analysis of proteinase K digests of Rho purified in DDM detergent micelles. (A) Schematic diagram of sample preparation and MS workflow. (B) UV-Vis spectrum of purified Rho in DDM. (C) Location of the chromophore-binding residue within helix VII of bRho, with labeled N^{ε}-retinyl-peptide fragments detected from the proteinase K digest. (D) Chromatographic separation of N^{ε}-retinyl-peptides from proteinase K digestion of purified Rho treated with $NaBH_4$ in *i*PrOH. (E-G) ESI-MS^1 spectra showing characteristic cleavage of retinyl cation (269 m/z) from precursor retinyl-peptide analyte, producing a product peptide peak. (H-J) MS^2 spectra of CID fragmentation of the product peptide ion for sequence determination.

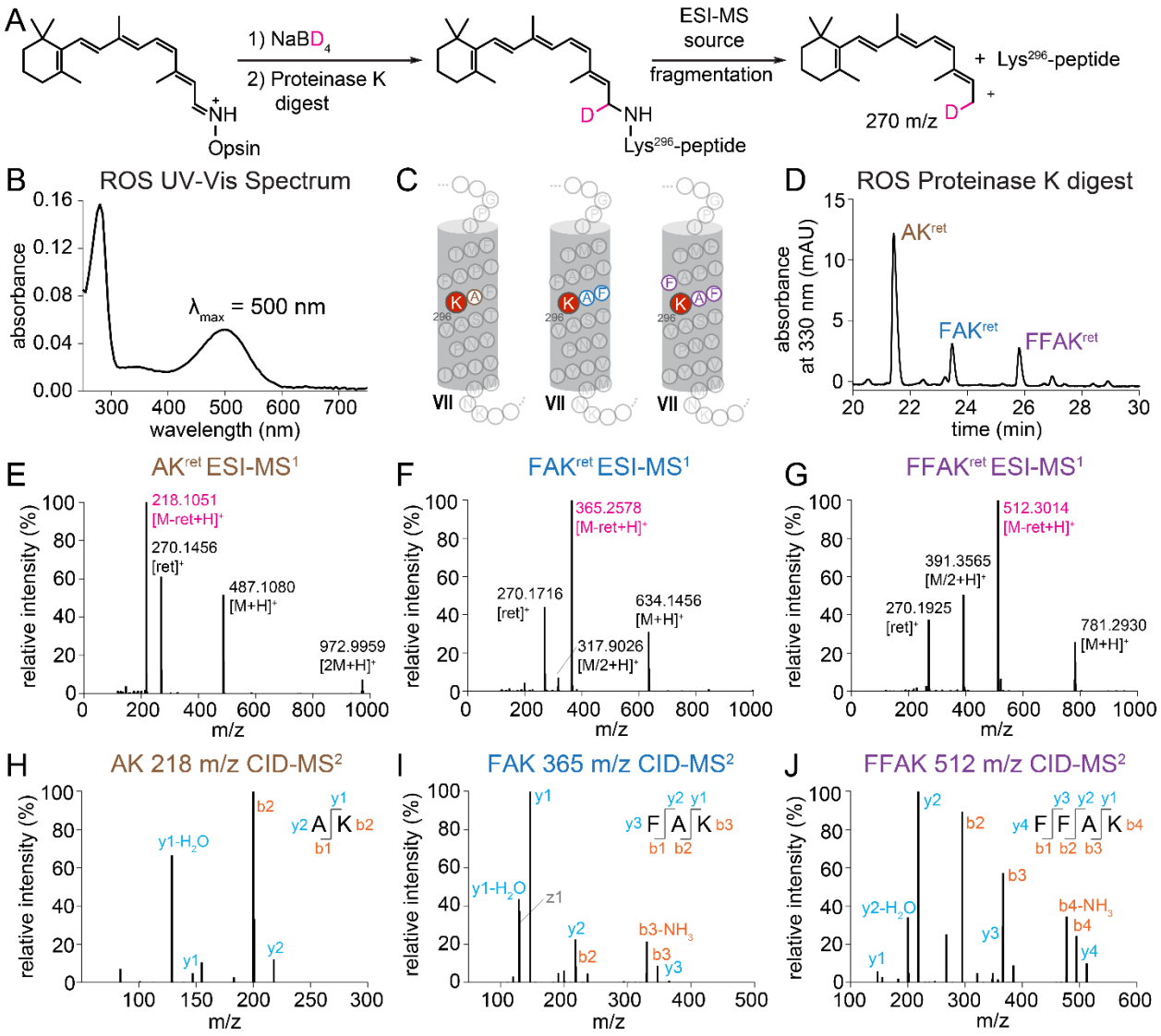

Figure S6. LC-MS/MS analysis of the proteinase K digest of NaBD$_4$-treated Rho from native membranes demonstrated retinylidene reduction and the retinyl cation fragmentation pattern. (A) Schematic diagram of sample preparation and MS workflow. (B) UV-Vis spectrum of Rho from ROS membranes solubilized in DDM. (C) Location of chromophore-binding digestion peptides within helix VII of bRho. (D) Chromatographic separation of N$^{\varepsilon}$-retinyl-peptide peaks from proteinase K digestion of Rho treated with NaBD$_4$ in *i*PrOH. (E-G) ESI-MS^1 spectra showing characteristic cleavage of C^{15}-D^1-retinyl cation (270 m/z) from precursor C^{15}-D^1-retinyl-peptide analyte, producing a product peptide peak. (H-J) MS^2 spectra of CID fragmentation of the product peptide ion for sequence determination.

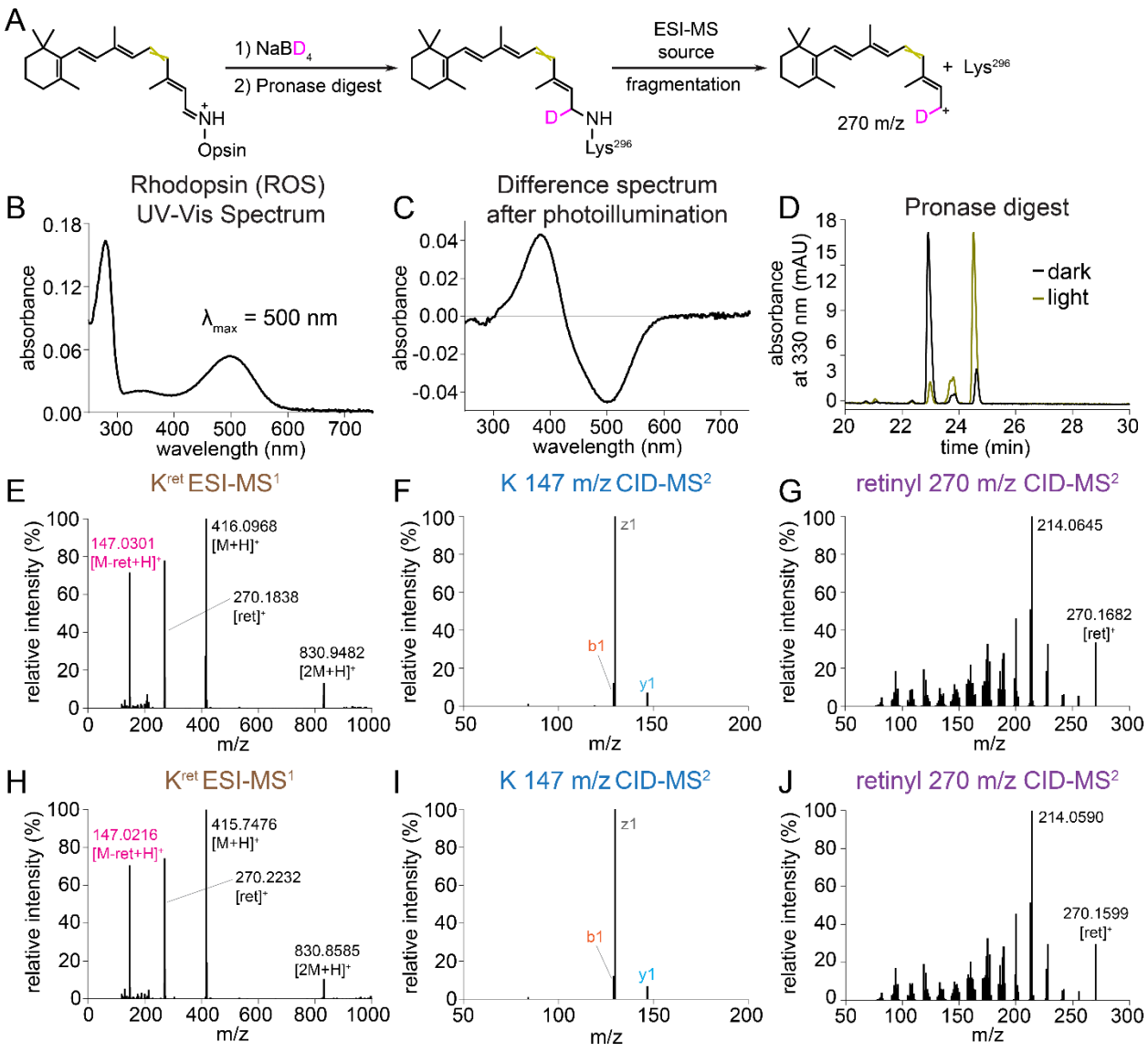

Figure S7. LC-MS/MS analyses of pronase digests of NaBD$_4$-treated Rho *vs.* Rho* from native membranes demonstrated RSB reduction and source fragmentation producing the C^{15}-D^1-retinyl cation. (A) Schematic diagram of sample preparation and LC-MS/MS workflow. (B) UV-Vis spectrum of Rho from ROS membranes solubilized in DDM. (C) Difference absorbance spectrum of DDM solubilized Rho *versus* Rho* in ROS membranes illuminated with 565 nm fiber light at 625 µW for 10 sec at 4 °C. (D) Chromatographic separation of N$^{\varepsilon}$-retinyl-Lys peaks from pronase digests of both Rho and Rho* from ROS membranes treated with NaBD$_4$ in *i*PrOH. (E-G) ESI-MS^1 spectra showing characteristic cleavage of C^{15}-D^1-retinyl cation (269 m/z) from precursor C^{15}-D^1-retinyl-Lys analyte (415 m/z), producing a product Lys ion (147 m/z). (H-J) MS^2 spectrum of CID fragmentation of the product Lys ion to confirm identity.

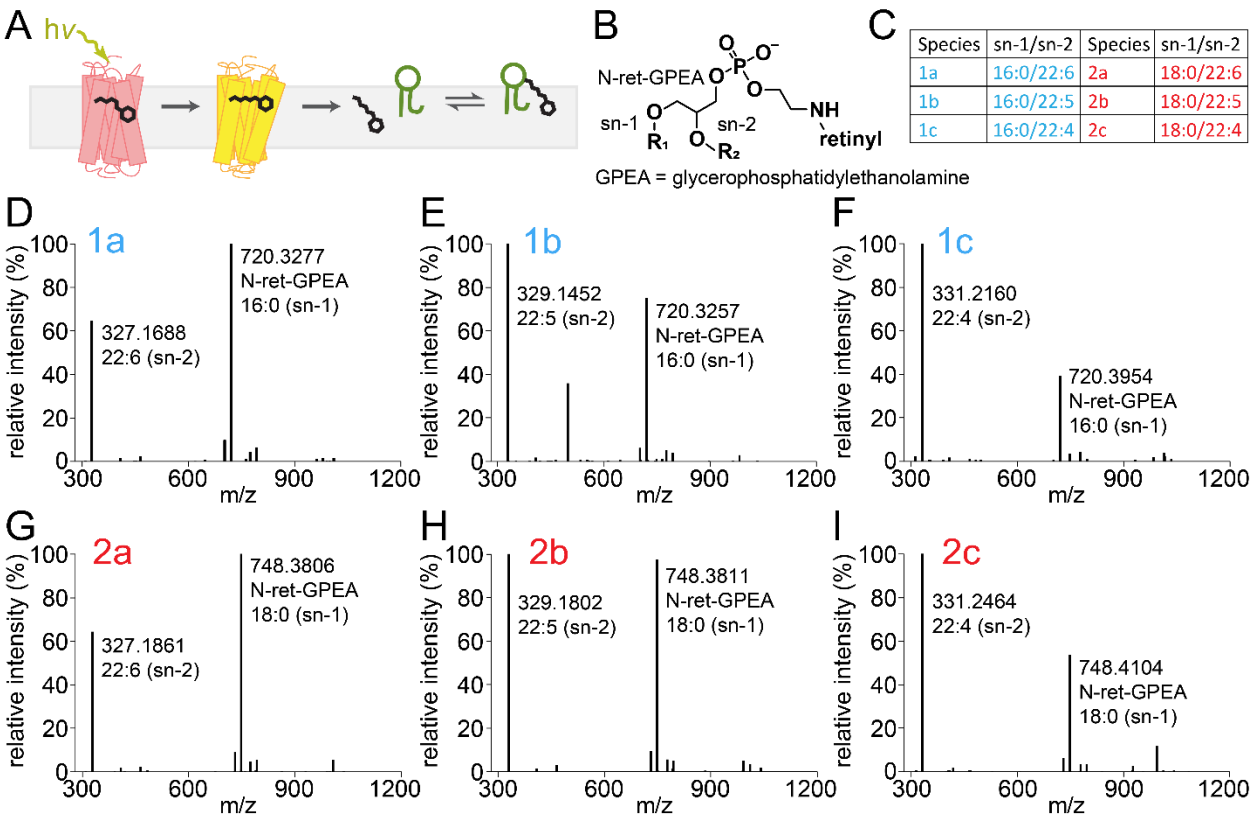

Species	sn-1/sn-2	Species	sn-1/sn-2
1a	16:0/22:6	2a	18:0/22:6
1b	16:0/22:5	2b	18:0/22:5
1c	16:0/22:4	2c	18:0/22:4

Figure S8. CID-MS^2 identification of N-ret-PE species. (A) Diagram of N-ret-PE formation after illumination of ROS membranes. (B) Chemical structure of N-ret-PEs. (C) Table of major N-ret-PE species found in the ROS membranes. (D-I) CID-MS^2 spectrum of each N-ret-PE with cleavage at the sn-2 position of the polyunsaturated acyl chain, using normalized collision energy of 35 eV.

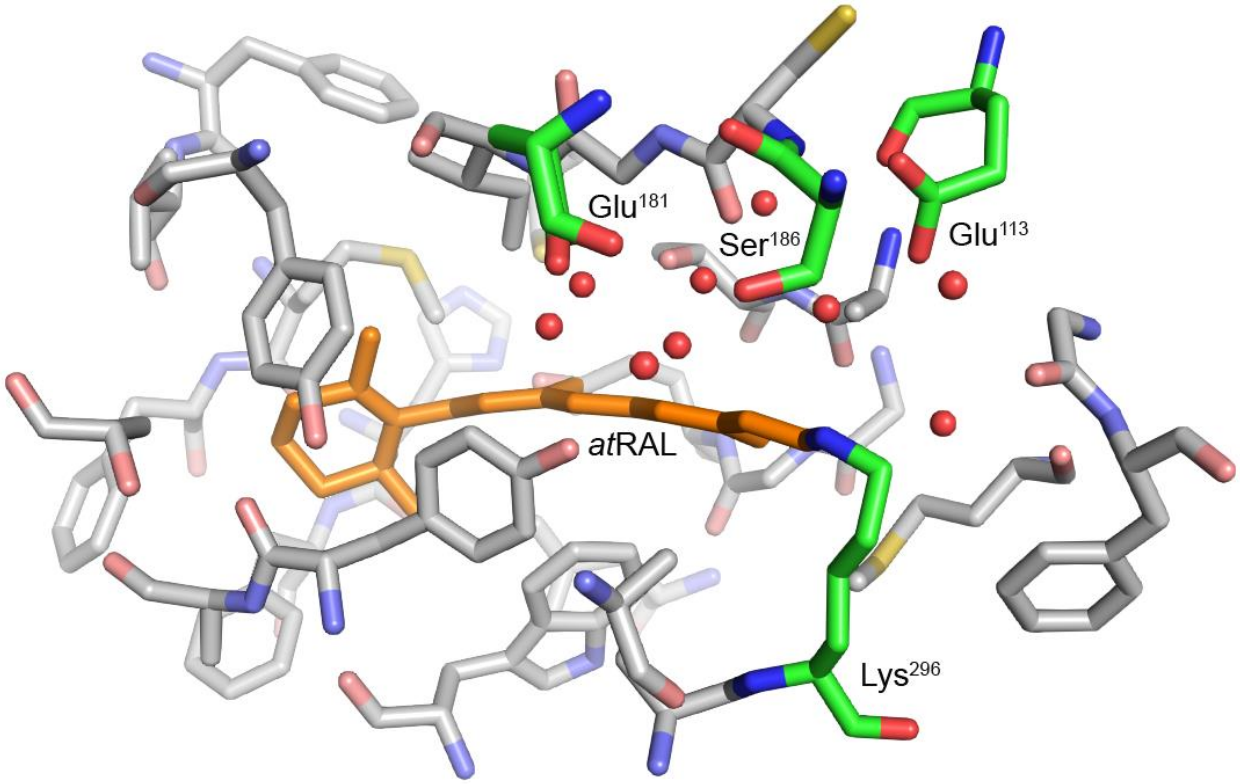

Figure S9. Molecular model used in quantum mechanical calculations. IIa structure and hydrogen atoms were omitted for clarity. Carbon atoms of the high-level QM1 region are highlighted in orange (a*t*RAL) and green (Glu^{113}, Glu^{181}, Ser^{186}, Lys^{296}). The region contains additionally nine water molecules (shown in red). Active site pocket (QM2) region includes the following residues: Met^{86}, Gly^{90}, Phe^{91}, Ala^{117}, Thr^{118}, Gly^{120}, Gly^{121}, Glu^{122}, Leu^{125}, Cys^{167}, Cys^{187}, Gly^{188}, Ile^{189}, Tyr^{191}, Phe^{203}, Val^{204}, Met^{207}, Phe^{208}, His^{211}, Phe^{212}, Trp^{265}, Tyr^{268}, Ala^{269}, Ala^{272}, Ala^{292}, Ala^{295}. The following atoms were kept frozen in the final H-saturated cluster: 3, 12, 21, 27, 193, 205, 217, 228, 235, 233, 264, 144, 149, 254, 181, 164, 173, 275, 168, 156, 316, 197, 129, 133, 121, 125, 239, 184, 289, 301, 306.

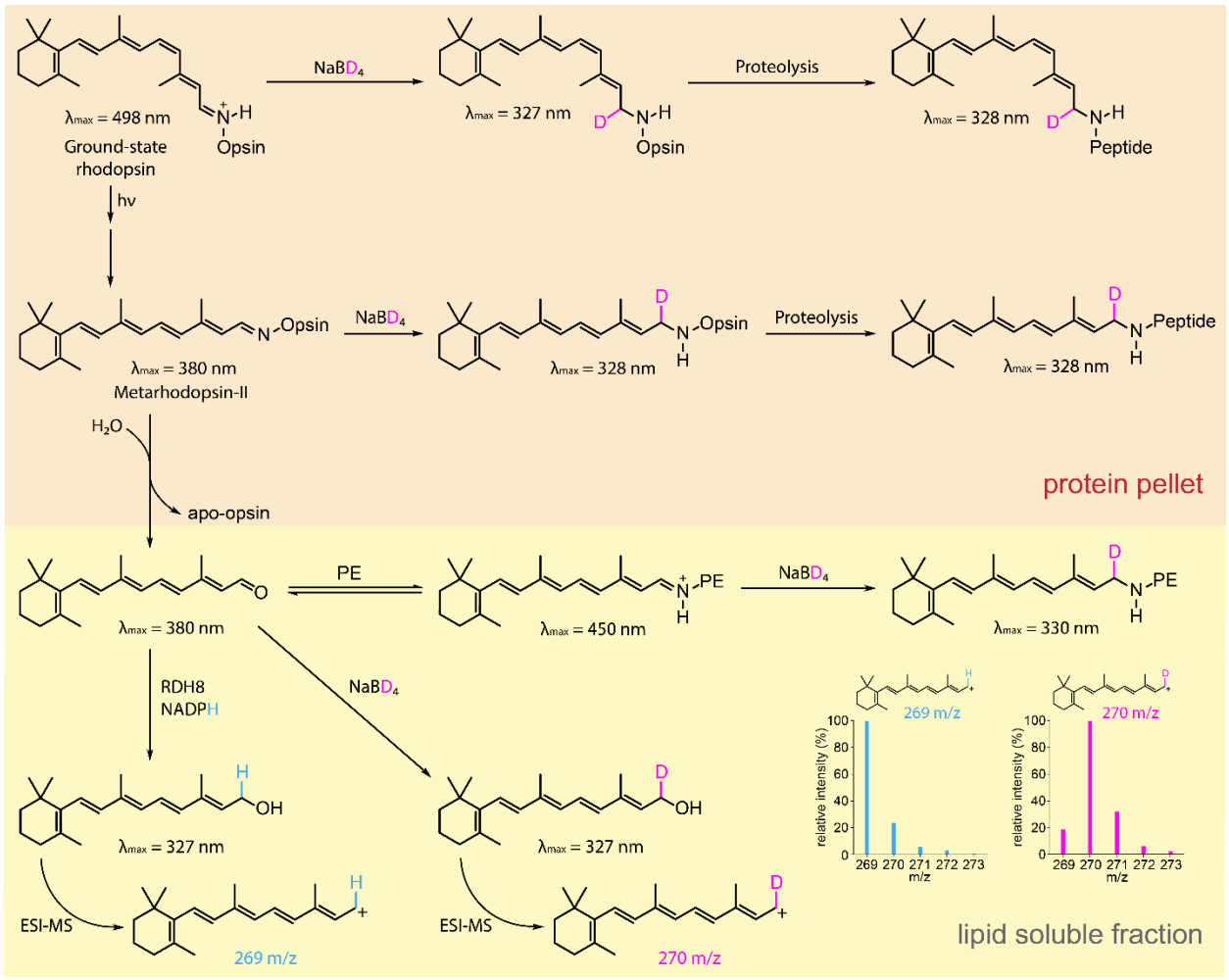

Figure S10. Strategy using $NaBD_4$ to monitor NADPH reduction by RDHs after Rho photoactivation. $NaBD_4$ mimics $NaBH_4$ in reducing Rho*-bound, PE-bound, and free a*t*RAL, with the only difference being the labeling all species with a deuterium. Reduction of a*t*RAL by NADPH and RDHs prior to $NaBD_4$ addition would produce non-deuterated a*t*ROL. The a*t*ROL and C^{15}-D^1-a*t*ROL can be detected by their ESI source-fragmentation retinyl-cation products. The ratio of a*t*ROL to C^{15}-D^1-a*t*ROL can be tracked, as well as the N-C^{15}-D^1-retinyl-Pes, to assess RDH activity on a*t*RAL produced from Rho* hydrolysis. Following LC-MS/MS analysis of the lipid-soluble fraction as described, Rho* hydrolysis kinetics could also be tracked by proteolysis and LC-MS/MS analysis of the protein pellet as described previously.

References

1. Kahremany S, Sander CL, Tochtrop GP, Kubas A, & Palczewski K (2019) Z-isomerization of retinoids through combination of monochromatic photoisomerization and metal catalysis. *Org Biomol Chem* 17(35):8125-8139.
2. Salom D*, et al.* (2006) Improvements in G protein-coupled receptor purification yield light stable rhodopsin crystals. *J Struct Biol* 156(3):497-504.
3. Choe HW*, et al.* (2011) Crystal structure of metarhodopsin II. *Nature* 471(7340):651-655.
4. Furness JW, Kaplan AD, Ning J, Perdew JP, & Sun J (2020) Accurate and Numerically Efficient r(2)SCAN Meta-Generalized Gradient Approximation. *J Phys Chem Lett* 11(19):8208-8215.
5. Weigend F & Ahlrichs R (2005) Balanced basis sets of split valence, triple zeta valence and quadruple zeta valence quality for H to Rn: Design and assessment of accuracy. *Phys. Chem. Chem. Phys.* 7(18):3297-3305.
6. Bannwarth C, Ehlert S, & Grimme S (2019) GFN2-xTB-An Accurate and Broadly Parametrized Self-Consistent Tight-Binding Quantum Chemical Method with Multipole Electrostatics and Density-Dependent Dispersion Contributions. *J Chem Theory Comput* 15(3):1652-1671.
7. Ehlert S, Stahn M, Spicher S, & Grimme S (2021) Robust and Efficient Implicit Solvation Model for Fast Semiempirical Methods. *J Chem Theory Comput* 17(7):4250-4261.
8. Neese F, Wennmohs F, Becker U, & Riplinger C (2020) The ORCA quantum chemistry program package. *J. Chem. Phys.* 152(22):224108.
9. Bannwarth C*, et al.* (2020) Extended tight-binding quantum chemistry methods. *WIREs Computational Molecular Science* 11(2).